NON-NEWTONIAN FLOW OVER THE TRAILING EDGE OF AN AEROFOIL

J. Sheridan[a], J. Wu[b], L. Pullum[b] and M. Welsh[b]
[a] Department of Mechanical Engineering, Monash University, Clayton 3168, Australia
[b] Division of Building, Construction and Engineering, CSIRO, Highett 3190, Australia

ABSTRACT

Results are presented from an experimental study of flow over a C4 aerofoil in a shear-thinning non-Newtonian flow. A digital particle image velocimeter (DPIV) was used to measure the instantaneous velocity field in the trailing edge region of the aerofoil placed at an angle of attack of 35 degrees. This flow field is relevant to that occurring around hydrofoils of agitators used for mixing slurries. It is shown that the Kutta condition was not satisfied at the trailing edge region. This implies a low lift force coefficient for the aerofoil. Features including velocity distributions and strain rate are presented based on measurement using the DPIV technique.

INTRODUCTION

Flow around an aerofoil is one of the most researched flow fields in fluid dynamics because of its important role in aerospace and hydraulic machinery. However most investigations in this field have been conducted in Newtonian fluids, particularly air. Non-Newtonian flow around aerofoils has been somewhat neglected in the literature. In addition to Rushton and pitch-bladed turbines, hydrofoils with aerofoil sections have been used extensively in modern mixing agitators (Oldshue 1983). Mixing in the mineral industry involving high concentration solid/liquid blending is a typical example of non-Newtonian flow around an aerofoil. An understanding of this flow is necessary to improve the design and operation of impellers in many mixing applications (Pullum *et al.* 1994).

This paper is a first step aimed at improving our understanding of this type of flow using the DPIV technique. The flow field in the trailing edge of a C4 aerofoil at three different velocities will be presented.

EXPERIMENTAL FACILITIES

A return-circuit water tunnel located at CSIRO, Highett, Australia was used for the experiments. The working section of the tunnel is 770 mm long, 244 mm high and 244 mm wide. The walls of the tunnel are made of transparent acrylic material. A C4 aerofoil with a chord of C = 130mm and thickness of 10%C was used for measurements described here.

A clear 0.1% Carbopol 940 solution was used as a test fluid. The solution is a visco-plastic non-Newtonian fluid which shows shear-thinning characteristics as graphed in

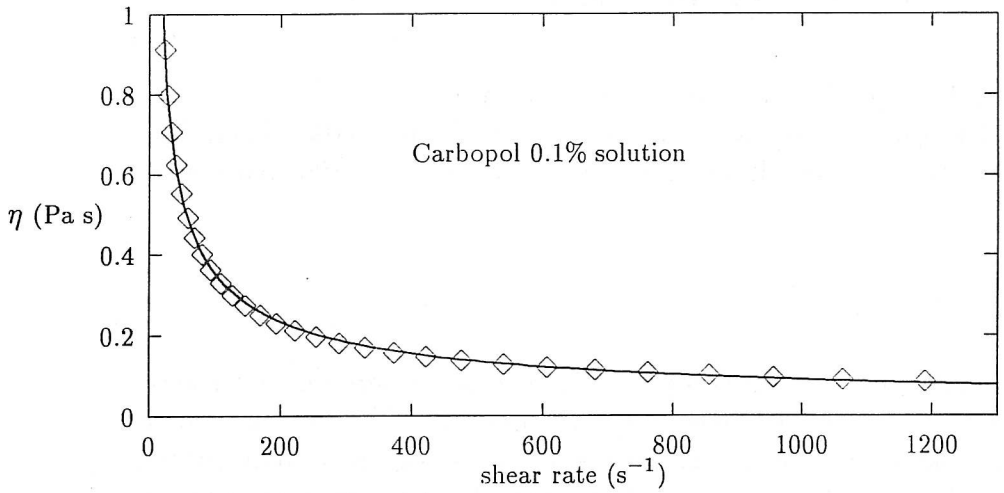

Figure 1: Apparent viscosity vs. shear rate for 0.1% Carbopol 940 solution.

Fig. 1. The rheological data is well described by the Herschel-Bulkley model and is fitted as shown below:

$$\eta = 1.514/\dot{\gamma} + 5.04\dot{\gamma}^{-0.585} \tag{1}$$

where η is the apparent viscosity and $\dot{\gamma}$ is the strain rate.

The flow was seeded with white 'Hollow Microsphere' glass beads with a mean diameter $< 30\ \mu m$. An 8W Argon-ion continuous laser beam was transmitted through a 50 μm diameter multi-mode optical fibre and spread into a light sheet using a cylindrical lens. The laser light was pulsed using a mechanical shutter installed in front of the fibre-optics input coupler. The light scattered from the particles in the laser sheet was recorded using a 'Videk' digital CCD camera with a spatial resolution of 1280 $\times$ 1024 pixels; the light intensity signal was digitised into 256 levels (8-bit) on a personal computer. A Silicon Graphic workstation was used to reduce the velocity field from the particle image using a digital PIV software system based on a Young's fringe method.

The principle behind the Young's fringe method was outlined in the early work of Barker and Fourney (1977). Basically, the pulsed particle displacement image in a small interrogation window is transformed into a fringe pattern (Young's fringe pattern) either optically, using a coherent laser beam, or digitally, using FFT computations. The digitised Young's fringe pattern is then processed to give an average velocity over the interrogation area. For more recent information in this field, the reader is referred to the reviews by Adrian (1991) and Buchhave (1992). In this study a digital PIV technique was used and its detailed description can be found in Wu *et al.* (1994). The uncertainty of the velocity measurement is estimated to be approximately 4% at the 95% confidence level when the interrogation window of size 48 $\times$ 48 pixels is used.

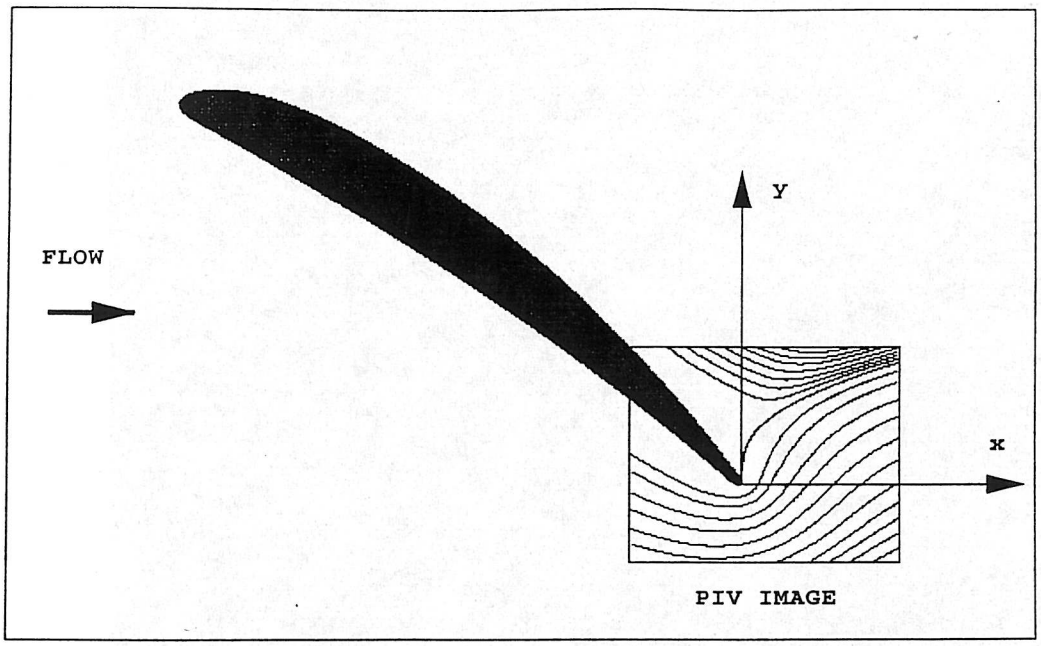

Figure 2: PIV measurement plane: the angle of attack 35 degrees, the curves inside the box are streamlines at $U_0 = 45.7mm/s$.

RESULTS AND DISCUSSIONS

The flow field in the trailing edge region of a C4 aerofoil was investigated as shown schematically in Fig. 2, where it is shown that the PIV image plane was 51.3 × 41.4 mm in size.

Typical particle images (with the laser sheet pulsed 5 times) are presented in Figs 3(a) and (b) for two freestream velocities. The instantaneous velocity vector field calculated from the particle images are presented in Figs 4(a) and (b). Flow from the high pressure side (bottom side) of the aerofoil turns around the tip of the trailing edge of the aerofoil. A stagnant flow region was formed on the top side of the aerofoil. Flow was found to be in a steady state and there was no recirculation or vortex shedding. The thickness of the stagnant region is reduced when the freestream velocity was increased from $U_0 = 45.7$ mm/s to 190 mm/s.

One important feature of this flow is that the Kutta condition is not satisfied. The direction of the flow leaving the trailing edge deviates from the orientation of the rear part of the aerofoil completely. The well-known starting vortex mechanism responsible for adjusting the circulation of an aerofoil to transfer a stagnation point to the trailing edge is non-existent. It is not entirely clear whether this is purely an effect of the Reynolds number being low or an effect caused by the non-Newtonian fluid characteristics. Nevertheless it is noted that the non-Newtonian characteristics tend to promote the formation of a stagnant region. The stagnant region enlarges when a reduction in shear rate causes an increase in viscosity which in turn produces a further reduction in local shear rate. It was observed during flow visualisation that a region of unsheared fluid existed because the local shear stress was less than the yield stress of the fluid. The formation of these regions

(a)

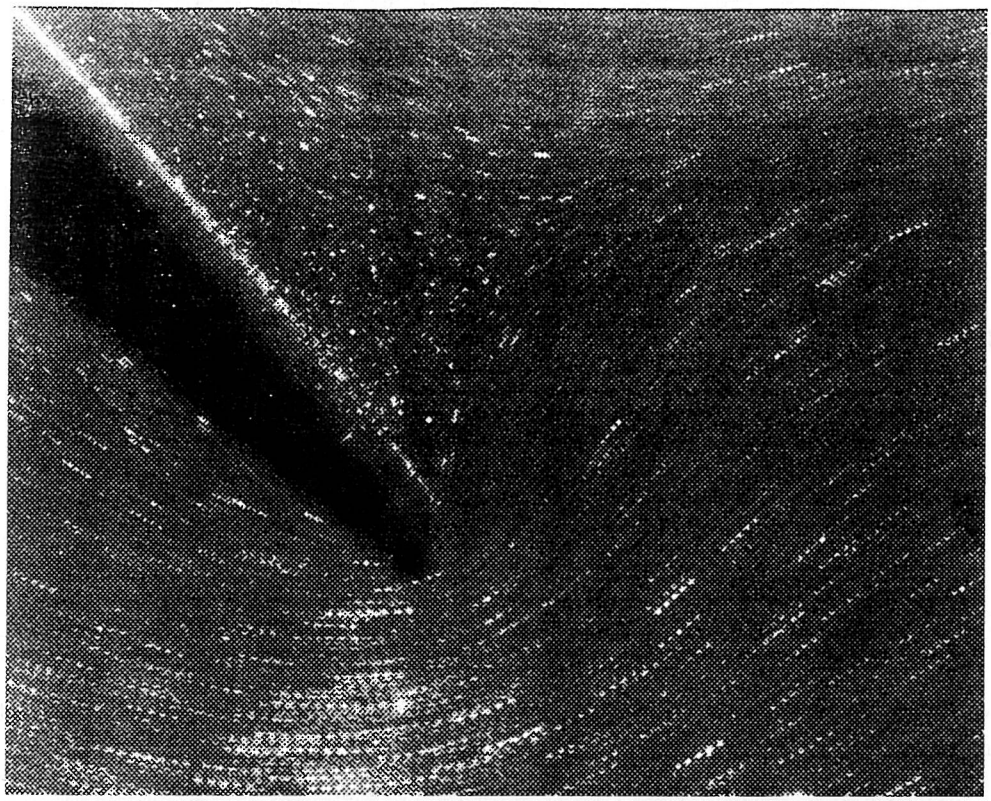

(b)

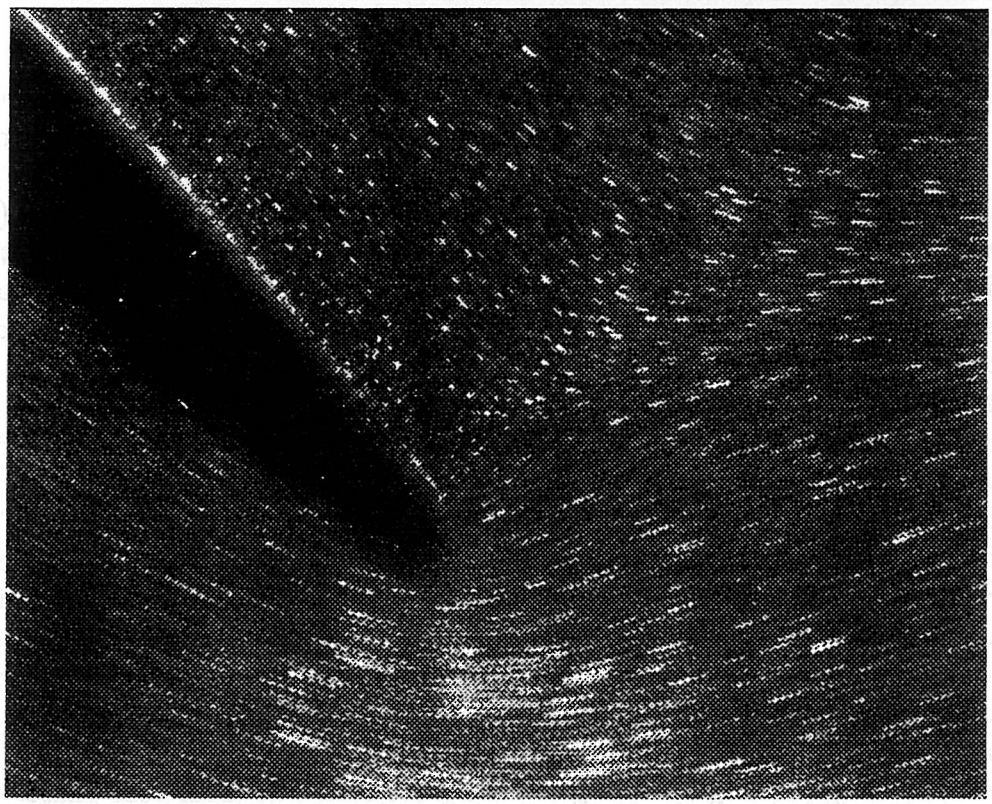

Figure 3: Flow in the trailing edge region of a C4 aerofoil placed at 35 degrees; flow from left to right: (a) $U_0 = 45.7$ mm/s, (b) $U_0 = 190$ mm/s.

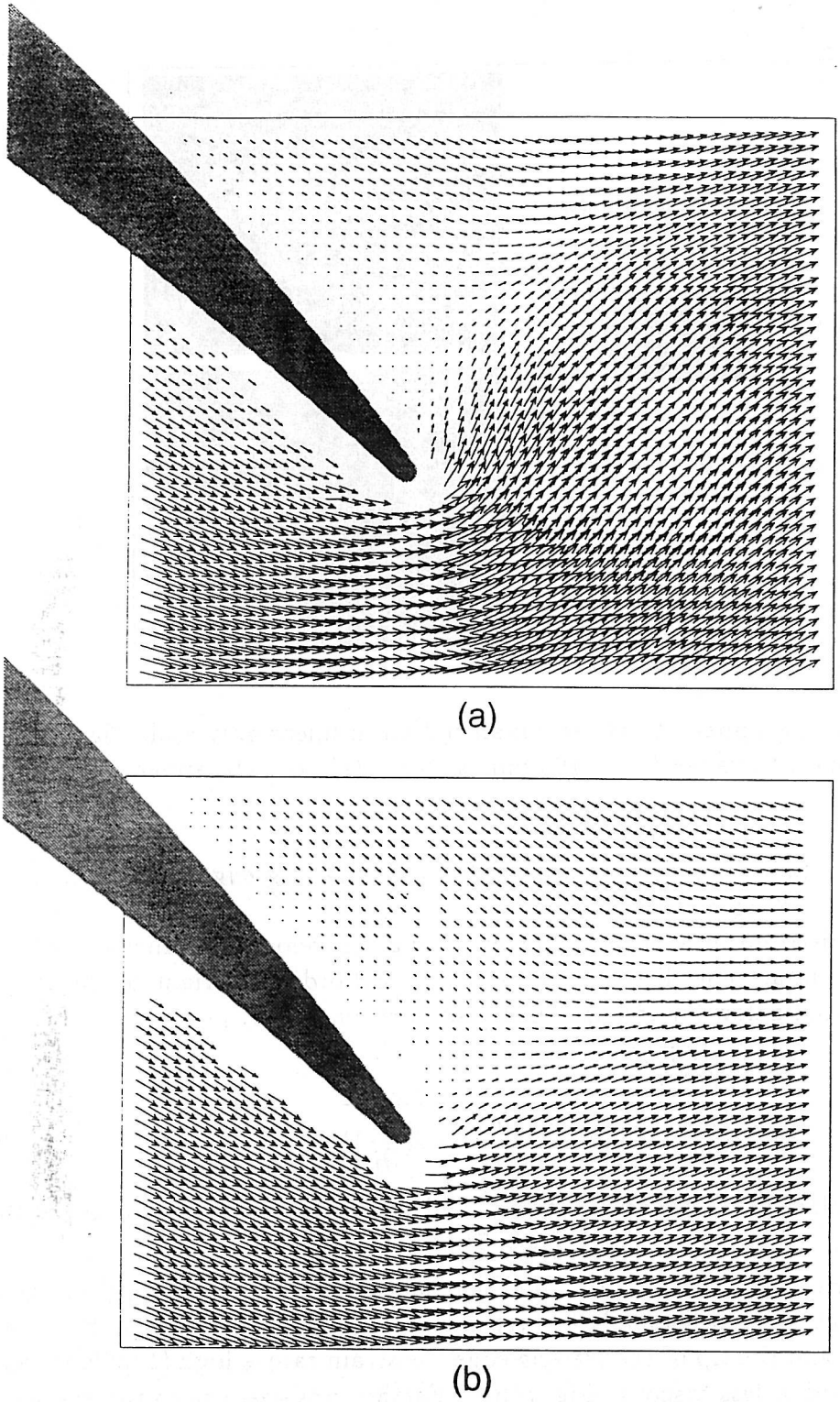

Figure 4: Instantaneous velocity vector field; flow from left to right: (a) $U_0 = 45.7$ mm/s, (b) $U_0 = 190$ mm/s. The length of velocity vectors is normalised with the freestream velocity.

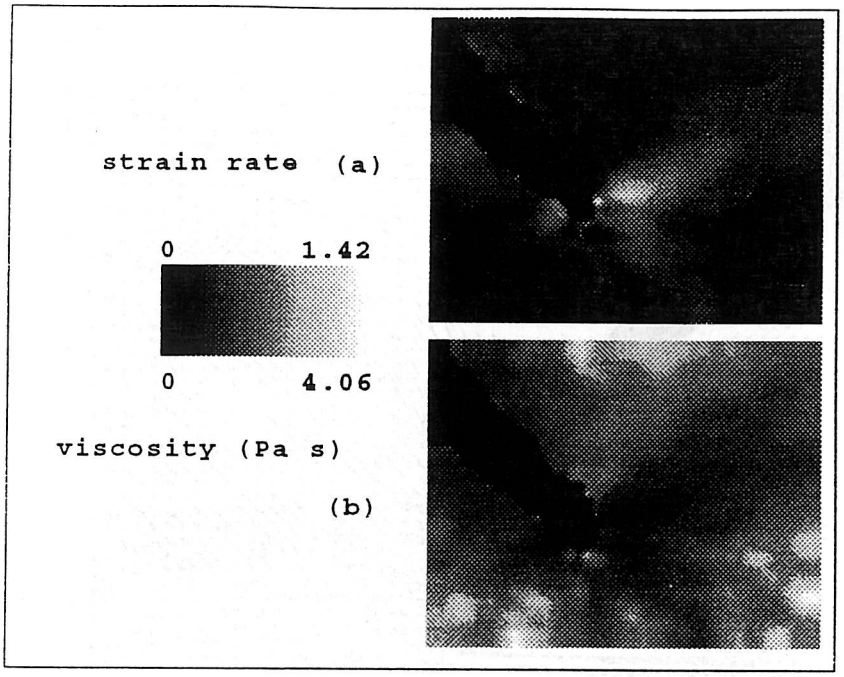

Figure 5: Strain rate and apparent viscosity distribution in linear gray-scale, light corresponds to high and dark to value; $U_0 = 190$ mm/s: (a) $\dot{\gamma}/(U_0/C)$, (b) apparent viscosity η.

produced a high 'resistance' for flow separating from the trailing edge, thus preventing the formation of the starting vortex.

The strain rate distribution can be found by evaluating velocity gradients from the velocity distribution data. The distribution of the second-order invariant of the strain rate tensor is calculated below for the present two-dimensional flow:

$$\begin{aligned}\dot{\gamma} &= \sqrt{2S_{ij}S_{ij}} \\ &= \sqrt{(\frac{\partial u}{\partial y} - \frac{\partial v}{\partial x})^2 + 2(\frac{\partial u}{\partial x})^2 - 2(\frac{\partial v}{\partial y})^2}\end{aligned} \tag{2}$$

where u and v are velocity components in the x- and y-direction respectively. S_{ij} is the strain rate tensor and defined as: $S_{ij} = \frac{1}{2}(\frac{\partial u_i}{\partial x_j} - \frac{\partial u_j}{\partial x_i})$

The $\dot{\gamma}$ and η distributions at $U_0 = 190$ mm/s are shown in Figs 5(a) and (b) in linear grey scale, where light grey corresponds to high and dark grey to low values. It is seen that immediately around the tip of the trailing edge the strain rate is high (Fig. 5(a)) and consequently that fluid is less viscous (Fig. 5(b)). Further upstream near the stagnant region, the strain rate is low as evident from the dark region shown in the figure. This implies the existence of a highly viscous region on the low pressure side of the aerofoil. It is hypothesised that an increase in viscosity in this low strain rate region inhibits the formation of the starting vortex and hence a violation of the Kutta condition.

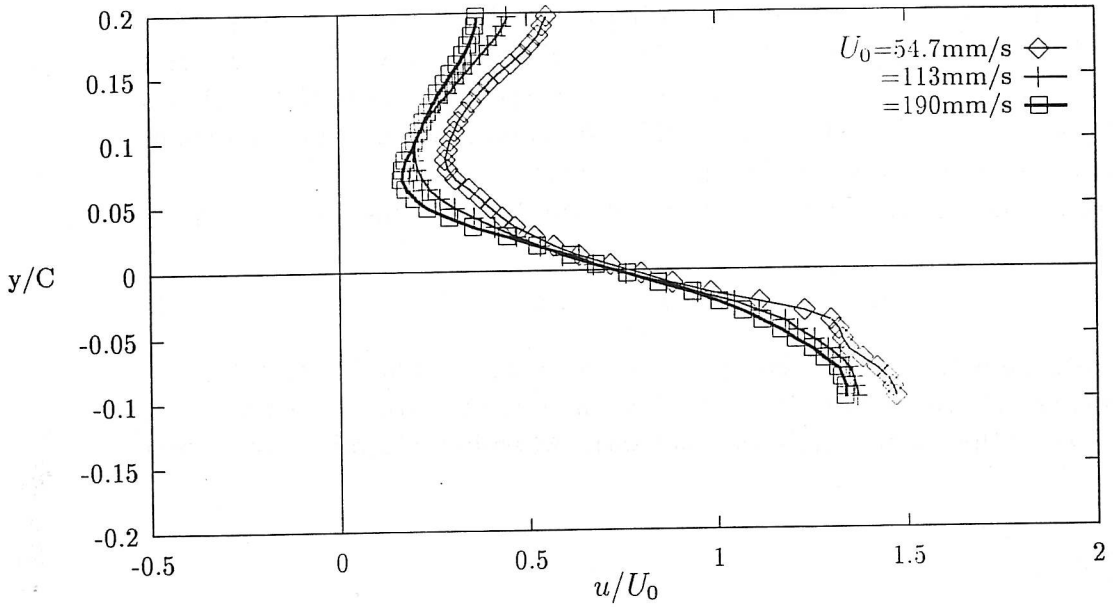

(a)

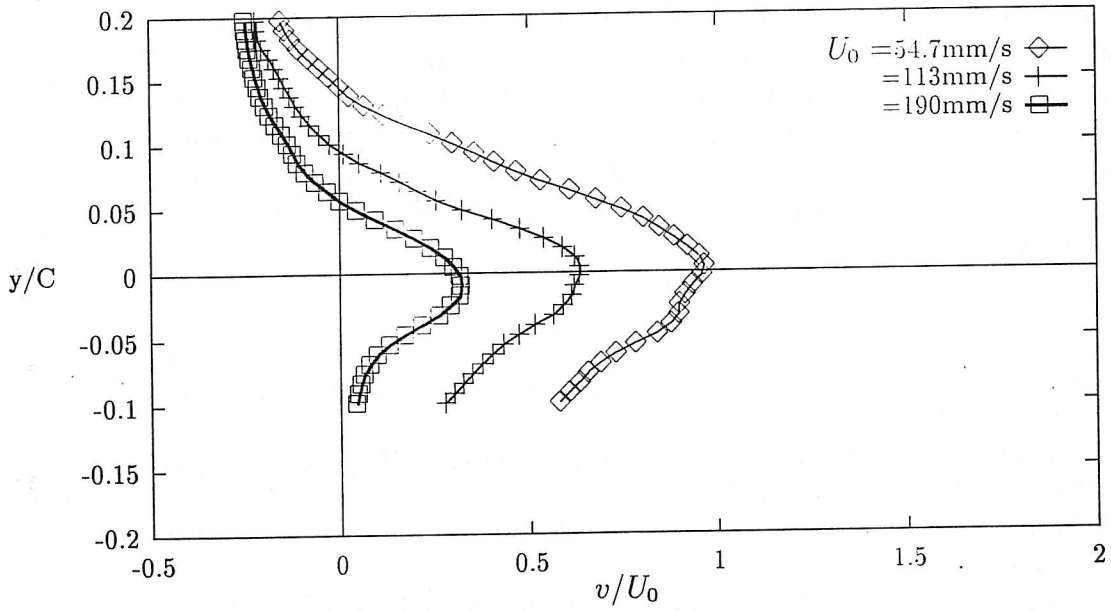

(b)

Figure 6: Velocity profile in the trailing edge region; C is the chord length of the aerofoil: (a) u velocity component, (b) v velocity component.

There is a large variation of velocity across the flow (in the y-direction) as shown in the velocity profile in Figs 6(a) and (b), taken 5 mm downstream of the trailing edge. The coordinate system is defined in Fig. 2. The y-coordinate is normalised with C (the chord), and the velocity is normalised by the freestream velocity U_0. It is seen that the minimum u (Fig. 6(a)) is located at $y/C \approx 0.07$ (corresponding to the location of the stagnation point), well above the trailing edge (at $y/C = 0$) for all three cases. Maximum velocity gradient occurs near y/C=0, i.e. near the trailing edge. Where it has been shown that a high strain rate region exists. Figure 6(b) shows that the cross-flow velocity component v peaks at the trailing edge, which is a violation of the Kutta condition.

In passing it can be shown, using a momentum balance, that the lift force generated by an aerofoil is:

$$L \approx -\rho \int_{-\infty}^{+\infty} uvdy + \int_{-\infty}^{+\infty} \tau_{xy} dy \tag{3}$$

where L is the lift force, ρ is the density and τ_{xy} is the shear stress. The integration is to be taken along a vertical line (parallel to the y-axis) downstream the trailing edge. In the present case $v >> 0$ since the Kutta condition is not satisfied and this implies a reduction in the lift force.

CONCLUSIONS

A digital PIV technique has been used successfully to investigate a non-Newtonian fluid flow around the trailing edge of a C4 aerofoil. Flow features including velocity and strain rate distributions are presented for a number of freestream velocities. A high strain rate region is identified near the tip of the trailing edge and a low strain rate zone further upstream (on the low pressure side of the aerofoil) is also identified. The existence of the latter implies high viscosity and the formation of resistance to flow recirculation which inhibits the starting vortex, leading to a violation of the Kutta condition. The work described here is a first step towards understanding the non-Newtonian viscous flows in impellers of various mixing agitators.

REFERENCES

Adrian, R. J., 1991, 'Particle imaging techniques for experimental fluid mechanics', *Ann. Rev. Fluid Mech.*, **23**, 261-304.

Barker, D. B. and Fourney, M. E., 1977, 'Measuring fluid velocities with speckle patterns', *Optics letters*, **1**, No.4, 135-137.

Buchhave, P., 1992, 'Particle image velocimetry — status and trends', *Experimental Thermal and Fluid Science*, **5**, 586-604.

Oldshue, J. Y., 1983, '*Fluid Mixing Technology*', Chemical Engineering McGraw-Hill Pub. Co..

Pullum, L., Welsh, M. C., Sheridan, J. and Wu, J., 1994, 'Sensitivity of the mixing of a yield stress fluid to agitator configuration', *The Australian Mixing Conference*, Newcastle, Australia, 6-1.

Wu, J., Sheridan, J., Soria, J. and Welsh, M., 1994, 'An investigation of unsteady flow behind a circular cylinder using a digital PIV method', *1994 ASME FED Summer Meeting.*